Development of snow accretion simulation method for electric wires in consideration of snow melting and shedding

Kazuto Ueno, Yuzuru Eguchi, Takashi Nishihara, Soichiro Sugimoto, Hisato Matsumiya
Central Research Institute of Electric Power Industry (CRIEPI)
k-ueno@criepi.denken.or.jp

***Abstract*: In order to quantitatively clarify the process from the start of snow accretion to overhead transmission lines until snow shedding, we have developed a numerical code, SNOVAL®(Ver.3) (Snow accretion simulation code for overhead transmission lines). SNOVAL consists of meteorological data as input, a snow accretion model, a thermodynamic model for snow melting, and a snow shedding model. In the snow accretion model, dynamic effect of an electric wire rotation by external moments due to gravitational and aerodynamic forces on snow deposit is considered. The shape of accreted snow produced by SNOVAL is not necessarily to maintain cylindrical shape as in simple cylindrical accretion models. In contrast to the existing snow accretion models in which the snow deposit is always oriented normal to the wind speed, SNOVAL is applicable to snow accretion on electric wires under calm to strong wind in any direction. In the thermodynamic model with heat exchanges between the air, electric wire and snow deposit, the liquid water content in the snow deposit is introduced by taking into account the melting of snow deposit as well as the melting of snowflakes prior to impact. The sticking efficiency (accretion factor) and density of the accreted snow in the snow accretion model are parameterized based on the liquid water content and the shape of accreted snow. In the snow shedding model, the adhesive force between the surface of electric wire and ice granules is estimated as a function of the liquid water content. Wet snow shedding is numerically evaluated based on the balance of forces and its related moments exerted on the accreted snow. SNOVAL is applied to natural wet snow accretion to conductor samplers supported by wires, and the quantitative comparisons between numerical and observational results are made.**

Keywords: Snow accretion simulation, Accretion factor, Liquid water content, Adhesive force, Snow shedding

INTRODUCTION

In order to prevent snow related damage to overhead transmission facilities, a great deal of research has been done to understand wet-snow accretion to overhead transmission lines and to improve the accuracy in predictions on accreted snow load. However, physical model explaining all processes from the start of snow accretion, growth, until snow shedding is still not satisfactory, research efforts continue in many countries [1-4]. On the other hand, computer aided simulations for snow accretion across the span of the conductor have been developed since 1970, taking into account the effect of conductor rotation on the snow accretion process [1,5]. CRIEPI also has developed a snow accretion simulation code, named SNOVAL(Ver.2), which can evaluate numerically the temporal change of three dimensional accreted snow shape, mass and electric wire rotation under calm to strong wind in any direction [6,7].

SNOVAL(Ver.2) has been improved to incorporate a model of snow accretion to electric wires and snow melting. This model enables us not only to calculate the liquid water content of snow deposit by taking into account the melting process due to heat exchanges between the air, electric wire and snow deposit, but also to give density of snow deposit and accretion factor based on the liquid water content. Adhesive force between the surface of electric wire and snow deposit is also estimated based on the liquid water content. Furthermore, a snow shedding model is incorporated in the improved version, in which the time of snow shedding is quantitatively evaluated based on the balance between the adhesive force and gravitational, aerodynamic forces exerted on snow deposit, or the balance of moments related to these forces. The extended version, SNOVAL(Ver.3), is thus able to reproduce the process from the start of snow accretion until snow shedding [8].

In this paper, we give a brief outline of physical models developed in [8] with some modifications of parameterization for density of snow deposit and accretion factor. Numerical results obtained from SNOVAL(Ver.3) are compared with observations for a wet snow event in Japan.

I. MODELS

As shown in Fig. 1, SNOVAL(Ver.3) is an extended version based on SNOVAL(Ver.2), and consists of an input of meteorological data of surface and atmosphere (top), model of snow accretion growth and wire rotation (left), model of snow accretion and melting (right), and model of snow shedding (bottom).

A. Dynamical model of snow accretion growth and electric wire rotation

Snow accretion growth and shape at the position (x, ψ) at time t is determined by solving the following equation of thickness $h(x, \psi, t)$ of snow layer attached to a smooth cylindrical conductor (Fig.2):

$$\frac{\partial h\,(x,\psi,t)}{\partial t} = -\frac{\sigma(t)(\mathbf{S}\cdot\mathbf{n_e})}{\rho_s(t)(\mathbf{N}\cdot\mathbf{n_e})} \quad (1)$$

where $\sigma(t)$ is the accretion factor (the fraction of snow that sticks to the snow deposit after collision), $\rho_s(t)$ the density of the accreted snow, and $\mathbf{n_e}$ and $\mathbf{N}$ the outward unit normal to the accreted surface and to the conductor, respectively. The quantities $\sigma(t)$ and $\rho_s(t)$ are unknown and need to be parameterized. $\mathbf{S} = G_0\mathbf{v_s}$ is the accretion intensity per unit area due to the mass concentration G_0 of falling wet snow in the air multiplied by impact speed of snowflakes $\mathbf{v_s}$. Here G_0 is given by

$$G_0 = \rho_w P(t) \times 10^{-3}/(600 v_f) \text{ for } P[\mathrm{mm/10min}] \quad (2)$$

where ρ_w is the density of water and v_f is the terminal speed of snowflakes corresponding to the precipitation rate P. Snowflakes follow rectilinear paths in the wind direction prior to impaction because of their large inertia. Therefore, $\mathbf{S} = G_0\mathbf{v_s}$ can be approximated as $\mathbf{S} = G_0\mathbf{v}$, where $\mathbf{v} = (v_x, v_y, v_z)$ is the wind velocity. Using the horizontal wind speed $w_v(t) = \sqrt{{v_x}^2 + {v_y}^2}$, wind direction $\theta_d(t)$ and azimuth θ_c (Fig.3), and

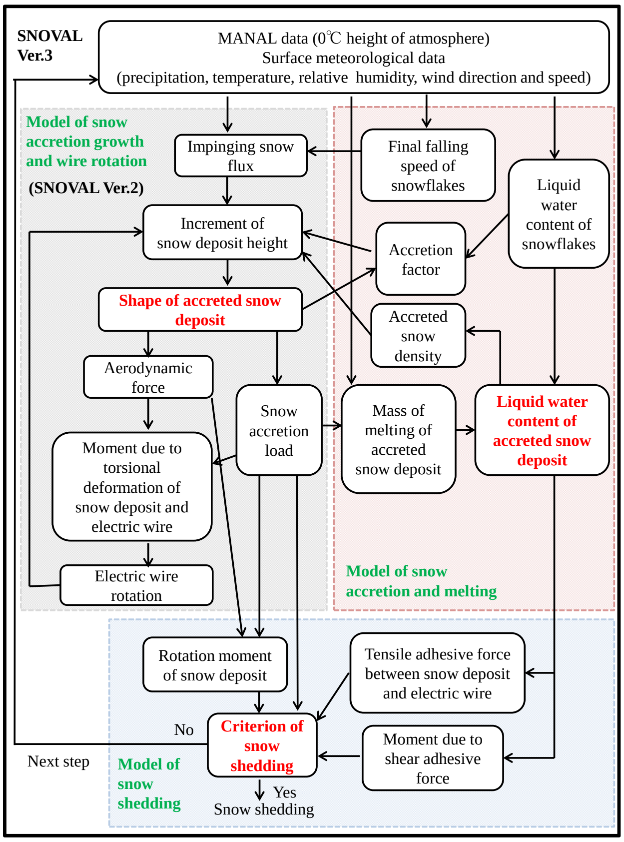

Fig.1. Framework of SNOVAL Ver.3.

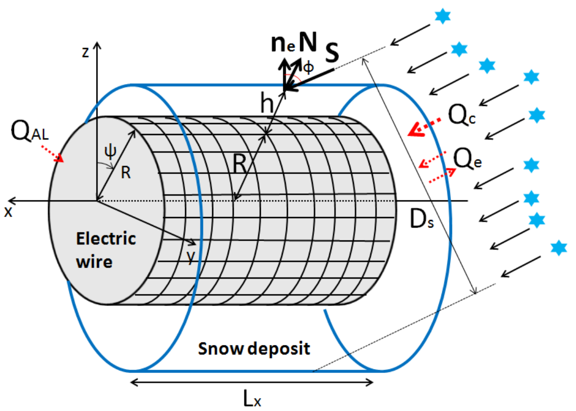

Fig.2. Snow accretion on a smooth cylindrical electric wire of finite length.

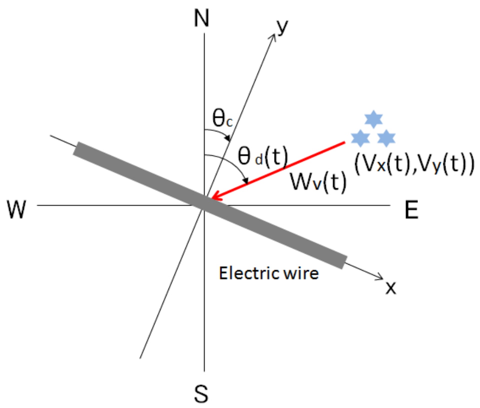

Fig.3. Wind direction relative to an electric wire.

considering the case of absence of up and down blow, $v_z = 0$, $\mathbf{S}$ can be expressed as

$$\mathbf{S} = \begin{pmatrix} S_x(t) \\ S_y(t) \\ S_z(t) \end{pmatrix} = G_0 \begin{pmatrix} -w_v(t)\sin(\theta_d(t)-\theta_c) \\ -w_v(t)\cos(\theta_d(t)-\theta_c) \\ -v_f \end{pmatrix} \tag{3}$$

The accumulated snow mass per unit length of a conductor with L_x in length is estimated from

$$m(t) = \frac{\rho_s(t)}{2L_x}\int_0^{L_x}\int_0^{2\pi}\left\{\left(R + h\,(x,\psi,t)\right)^2 - R^2\right\}d\psi dx \tag{4}$$

The equation for the rotation angle φ due to the torsional deformation of electric wire is given by

$$I\frac{\partial^2\varphi}{\partial t^2} = GJ\frac{\partial^2\varphi}{\partial x^2} + M_s' + M_w' \tag{5}$$

where I is the moment of inertia of electric wire and accreted snow, G the shear modulus and J the polar moment of inertia. M_s' and M_w' are moments due to gravitational and aerodynamic forces exerted on accreted snow, respectively. Since M_s' and M_w' depend on φ, (5) is a nonlinear equation with respect to φ.

B. *Snow deposit melting*

The rate of production of melt water within snow deposit is

$$\frac{dm_w(t)}{dt} = \left(Q_c(t) + Q_e(t) + Q_{Al}(t)\right)/L_f \tag{6}$$

where $m_w(t)$ is the mass of melt water per unit length and L_f the latent heat of fusion. $Q_c(t)$ is the convective heat flux from the airstream:

$$Q_c(t) = h_c(t)(T_a(t) - T_s) \times l(t) \tag{7}$$

where T_a is the air temperature, T_s the fusion temperature (0℃ for wet snow deposit mixing of ice and water), and $l(t)$ arc length of the outside of accreted snow. h_c is the heat transfer coefficient defined by

$$h_c(t) = K_a Nu(t)/D_s(t) \tag{8}$$

where K_a is the thermal conductivity of air, $Nu(t)$ the Nusselt number averaged over the circumference of the snow deposit, and D_s the distance of cross section of the snow deposit perpendicular to the snowflake impact speed (Fig.2). Using the Reynolds number defined by $Re(t) = D_s(t)|v_y(t)|/\nu_a$ with the kinematic viscosity of air ν_a, the following $Nu(t)$ is employed:

$$Nu(t) = \begin{cases} 0.891Re^{0.296} & (0.1 \le Re < 1) \\ 0.891Re^{0.330} & (1 \le Re < 4) \\ 0.821Re^{0.385} & (4 \le Re < 40) \\ 0.615Re^{0.466} & (40 \le Re < 4{,}000) \\ 0.174Re^{0.618} & (4{,}000 \le Re < 40{,}000) \\ 0.0239Re^{0.805} & (40{,}000 \le Re < 250{,}000) \end{cases} \tag{9}$$

$Q_e(t)$ is the evaporation/condensation heat flux for the accretion surface:

$$Q_e(t) = \frac{0.622h_c(t)L_e\left(\frac{RH(t)}{100}e_w(T_a(t)) - e_w(T_s)\right)}{C_p \times P_a} \times l(t) \tag{10}$$

where $RH(t)$ is the relative humidity, L_e the latent heat of evaporation over water, C_p the specific heat of air at constant pressure, P_a the atmospheric pressure, and $e_w(T)$ the saturation vapor pressure at temperature T[℃],

$$e_w(T) = 6.112 \times 10^{7.5T/(T+237.3)} \tag{11}$$

$Q_{Al}(t)$ is heat transfer from the environment by conduction across the conductor to the root of snow deposit:

$$\begin{aligned} Q_{Al}(t) &= -K_{Al}\int_{\psi_1}^{\psi_2}\left.\frac{\partial T}{\partial r}\right|_{r=R} R d\psi \\ &= h_c(t)(T_a(t) - T_0) \times \tilde{l}(t) \end{aligned} \tag{12}$$

where K_{Al} is the thermal conductivity of Aluminum, T_0 the temperature of the surface of electric wire, and $\tilde{l}(t)$ arc length of electric wire exposed to the atmosphere. Since the thermal conductivity of Aluminum is very large compared to that of air, it is a good approximation to put $T_0 = 0$℃ during snow accretion.

C. *Liquid water content*

The liquid water content (LWC) of accreted snow is defined as follows:

$$\Lambda(t) = \frac{\int_0^t \lambda(t)dm(t)}{m(t)} + \frac{m_w(t)}{m(t)} \tag{13}$$

where λ is the LWC of snowflakes before impact. The first term is the ratio of total mass of water due to snowflakes before impact to the mass of snow deposit, and the second term is the ratio of the mass of melt water produced form (6) to the mass of snow deposit. λ is calculated based on a micro-physical model of melting of snowflakes in the atmosphere, in which the effects of air temperature, relative humidity, and snowflakes size and density on the process of melting of snowflakes is estimated [9].

D. *Density of accreted snow and snow accretion factor*

Taking into account that the density of wet snow is closely related to wind speed [2,3] and the LWC of snow sample [10], we parametrize the density of accreted snow in terms of these variables:

$$\rho_s(t) = \frac{\rho_0 + \frac{550c}{550-\rho_0}|v_y|}{1+\frac{c}{550-\rho_0}|v_y|} \times (1 + \Lambda(t) + \Lambda(t)^2 + \cdots)$$
$$= \frac{\rho_0 + \frac{550c}{550-\rho_0}|v_y|}{1+\frac{c}{550-\rho_0}|v_y|} \times \frac{1}{1-\Lambda(t)} \qquad (14)$$

where $|v_y|$ is wind speed perpendicular to electric wire and snow deposit and $c = -\rho_0/25 + 35$. c was determined from the fact that the slope $d\rho_s/d|v_y|$ gradually decreases as ρ_0 increases in the experiment [11] (Fig.4). In case of dry density of $\Lambda = 0$ and $|v_y| = 0$, (14) gives ρ_0 which must be determined according to local conditions [4]. As $|v_y|$ increases, the first term of (14) approaches $550[kg/m^3]$ at which snow densification due to rearrangement of ice particle changes to that due to both rearrangement and plastic deformation. Furthermore, the first term of (14) gives approximately $\rho_0 + b|v_y|$ for small $|v_y|$, where b is the slope in the vicinity of $|v_y| = 0$ in Fig.4. This linear dependence of density on wind speed was adopted by many authors [1-4]. The second term of (14) comes from the experimental fact that the density increases as Λ increases [10]. Λ increases with increasing temperature, relative humidity, falling snowflakes speed, wheras Λ decreases with increasing precipitation rate and wind speed. In particular, Λ is very sensitive to temperature variation [8].

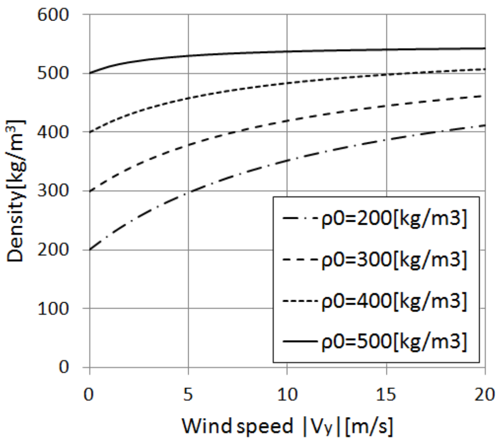

Fig.4. Dependence of the first term of (14) on the wind speed $|v_y|$ for various ρ_0.

We propose a local accretion factor which is a function of both meteorological conditions and the shape of three-dimensional snow accumulation:

$$\sigma(t) = \begin{cases} \dfrac{1+\cos\{10.5(\lambda(t)-0.1)\}}{2\left(\sqrt{1+(|v_y|/v_f)^2}\right)^A} \times \left(\dfrac{-\mathbf{S}\cdot\mathbf{n_e}}{|\mathbf{S}|}\right)^{\alpha(t)} & (-\mathbf{S}\cdot\mathbf{n_e} > 0) \\ 0 & (-\mathbf{S}\cdot\mathbf{n_e} < 0) \end{cases} \qquad (15)$$

The numerator of the first term of (15) achieves a maximum at $\lambda = 0.1$ and this is based on the idea that the accretion factor σ

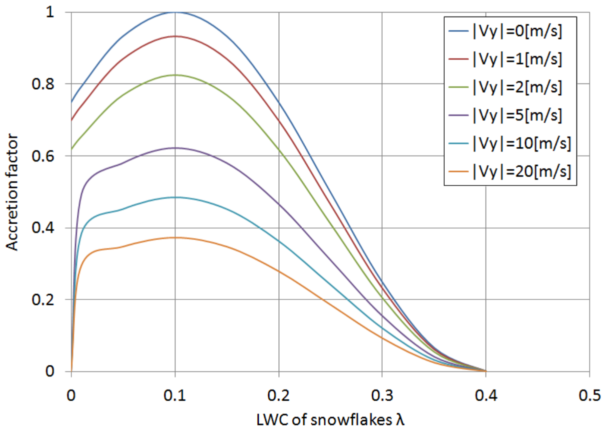

Fig.5. The first term of snow accretion factor (15) as a function of LWC of snowflakes for various wind speed $|v_y|$ [m/s].

is highest at a LWC of incoming snowflakes corresponding to the stickiest snow [4]. In case of dry snow, it is observed that snow accretion does not occur if $|v_y|$ is greater than 3[m/s][12] and hence $\sigma = 0$ in the vicinity of $\lambda = 0$ (Fig.5).

The second term of (15) is powers of a cosine $\cos\emptyset = -\mathbf{S}\cdot\mathbf{n_e}/|\mathbf{S}|$, where $\emptyset$ is the angle between the impacting trajectory and the normal to the surface of the snow deposit (Fig.2). This factor means that the probability of snow accretion is highest at the stagnation point (line) of snow deposit where shear force due to wind is zero and adhesive force between snow particles is dominant. On the other hand, far from the stagnation point (line), when shear stress is over adhesive force, the probability of the exfoliation of snow particles is high and then the accretion factor is decreased. Using the cosine low proposed by Poots [1], i.e. $\alpha = 1$, however, the calculated accreted mass underestimates the observations when the wind speed is small. On the other hand, when the wind speed is over $15[m/s]$, the calculated accreted mass overestimates the observations [12]. This suggests that the accretion factor is not necessary to obey the cosine law, and hence we propose the dependence of α on wind speed and diameter of snow deposit such that

$$\alpha(t) = B|v_y|^{1.5} D_s^{0.5} \qquad (16)$$

which comes from the fact that shear force due to wind around the surface of snow deposit is proportional to $|v_y|^{1.5} D_s^{0.5}$ [13]. As α increases, the second term of (15) leads to more streamline shapes in contrast to the bluff shapes (Fig.6). The effect of wind speed on the accretion factor σ is controlled by the factor A in the denominator of the first term of (15) and B in (16). The latter does not exist in the cylindrical-sleeve accretion models [1-4]. We employ an empirical calibration method in finding the appropriate values of A and B, allowing for the best agreement between calculated and observed mass of snow deposit. Applying to some Japanese wet snow events, the best agreement was found with $A = 0.38$ and $B = 0.15$. The value of A is close to 0.4 used in a cylindrical-sleeve accretion model [4].

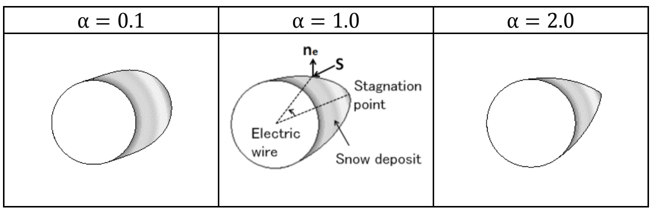

Fig.6. Accreted snow shapes for different α.

E. *Wet snow shedding*

Gravitational and aerodynamic forces exerted on snow deposit per unit lengh are, respectively,

$$f_g(t) = mg \quad (17)$$

$$f_w(t) = \frac{1}{2}\rho_a|v_y(t)|^2 C_d D_s(t) \quad (18)$$

where ρ_a is the air density and C_d the drag coefficient. Integrating the component of an infinitesimal tensile adhesive force parallel to the gravity over the surface between the electric wire and snow deposit (dashed red line in Fig.7 (a)), the total tensile adhesive force is

$$f_{tad}(t) = \int_{\pi/2}^{\psi_0} \sigma_{tad}(t)\cos(\pi-\psi)\,Rd\psi \quad (19)$$

where R is the radius of electric wire and the tensile adhesive strength σ_{tad} depends on the LWC and density of snow deposit as well as the surface roughness of electric wire. Once the lower part of the electric wire is completely covered with snow, ψ_0 in (19) is $3\pi/2$ and $f_{tad}(t) = \sigma_{tad}(t) \times 2R$. According to the experiments [10,14,15], σ_{tad} has a maximum $(\sigma_{tad})_{max}$ at a LWC of snow sample, which is around $\Lambda = 0.1\sim0.2$. However, it should be noted that $(\sigma_{tad})_{max}$ varies depending on the strength of initial compression force applied to the snow sample [15] and increases as the initial compression force increases. We employ the following σ_{tad} obtained for a small initial compression force [14,15],

$$\sigma_{tad} = \begin{cases} (10.0(\sigma_{tad})_{max} - 278.0)\Lambda + 27.8 & (0.0 \le \Lambda < 0.1) \\ -90.0\Lambda + (\sigma_{tad})_{max} + 9.0 & (0.1 \le \Lambda < 0.3) \\ -1045.5\Lambda + (\sigma_{tad})_{max} + 295.5 & (0.3 \le \Lambda < 0.4) \\ 0 & (0.4 \le \Lambda \le 1.0) \end{cases} \quad (20)$$

Figure 8 shows that σ_{tad} increases as Λ increases when $\Lambda < 0.1$ and achieves a maximum $(\sigma_{tad})_{max}\sim350[\mathrm{N/m^2}]$ at $\Lambda = 0.1$, and then gradually decreases as Λ increases, and finally $\sigma_{tad} = 0$ when $\Lambda > 0.4$. The criterion of snow shedding corresponding to the shape of accreted snow in Fig.7(a) is that gravitational force exceeds the tensile adhesive force,

$$f_g(t) > f_{tad}(t) \quad (21)$$

The moment due to gravity and wind force are, respectively,

$$M_g(t) = f_g r_{cg}\sin\theta_{cg} \quad (22)$$

$$M_w(t) = -f_w r_{cg}\cos\theta_{cg} \quad (23)$$

and we denote their sum as $M_{gw}(t)$, where r_{cg} is the center of

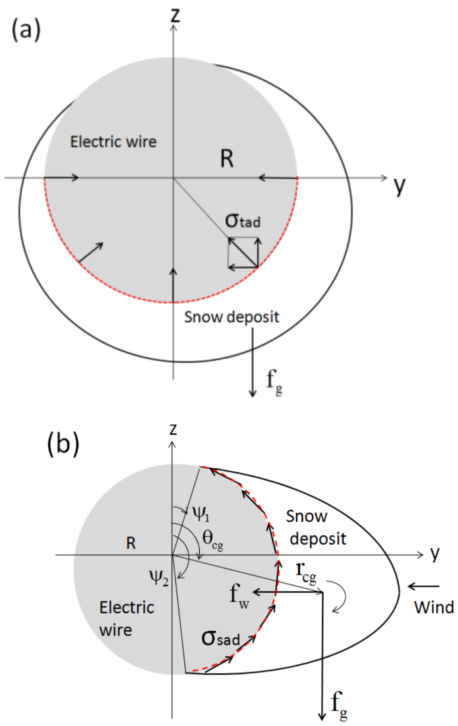

Fig.7. Snow shedding for different shape of accreted snow.

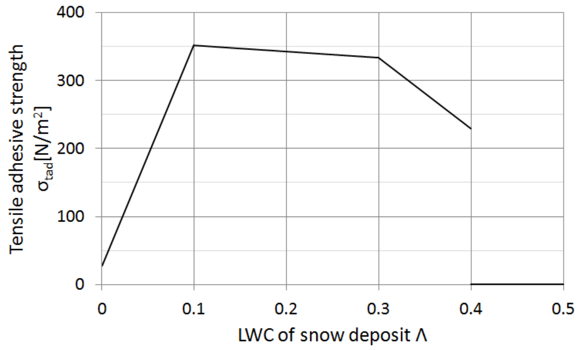

Fig.8. Tensile adhesive strength as a function of LWC of snow sample.

gravity of snow deposit and θ_{cg} is the angle from the zenith of electric wire and snow deposit (Fig.7(b)). Integrating shear adhesive strength σ_{sad} along the surface between the electric wire and snow deposit (dashed red line in Fig.7 (b)), the moment due to shear adhesive strength is

$$M_{sad}(t) = R\int_{\psi_1}^{\psi_2} \sigma_{sad}(t)Rd\psi \quad (24)$$

We assume that the dependence of σ_{sad} on LWC of snow deposit has a similar behaviour as that of the tensile adhesive strength σ_{tad}. However, its maximum $(\sigma_{sad})_{max}$ is different from $(\sigma_{tad})_{max}$. Since the tensile strength does not exceed twice the shear strength for most other materials, we assume that $(\sigma_{tad})_{max}/2 \le (\sigma_{sad})_{max} < (\sigma_{tad})_{max}$. The criterion of snow shedding corresponding to the shape of accreted snow in Fig.7(b) is that the moment due to gravity and wind force exceeds the moment due to shear adhesive force,

$$M_{gw}(t) > M_{sad}(t) \quad (25)$$

The time of wet snow shedding is numerically determined from the point where either (21) or (25) is satisfied. Here, we treat $(\sigma_{tad})_{max}$ and $(\sigma_{sad})_{max}$ as parameters and investigate the effect of these parameters on snow shedding time.

II. RESULTS AND DISCUSSION

We installed conductor samplers with different size, torsional stiffness, and orientation in Kushiro, where is located at east area of Hokkaido island in Japan, and have continued observations to clarify meteorological condition for wet snow events since 2010. Figure 9 shows the snow accretion process on different conductor samplers for a wet snow event at Kushiro on April 21, 2013. Each edge of a conductor sampler is supported by a short wire whose length and thickness control conductor rotation. The torsional spring constant k_s for sampler conductors is given by $k_s = 4GJ \times L_x/L^2$ so that the torsion of conductor sampler is equivalent to that in the middle of the span of actual transmission lines [16]. Here GJ is the torsional stiffness of actual electric wire with the same size as sampler conductor, L_x a half of length of conductor sampler, and L a half of span length equivalent to actual transmission line. Table 1 shows the specification of sampler conductors in Fig.9 and the value of a half of k_s for each conductor sampler is indicated.

The meteorological data on April 21, 2013 is shown in Fig. 10. Temperature, relative humidity, wind speed and direction were obtained at the observational location, whereas precipitation was observed at the weather station in the neighbourhood of the observational location. Precipitation was observed from 14:50 at both the weather station and the observational location. However, snow accretion to conductor samplers started at 15:40 after which temperature and relative humidity appropriate for snow accretion continued until 22:00. During this wet snow event, wind speed varied in the range 2~7[m/s], wind direction was almost perpendicular to conductor samplers, and mean precipitation rate was 0.6 [mm/10min].

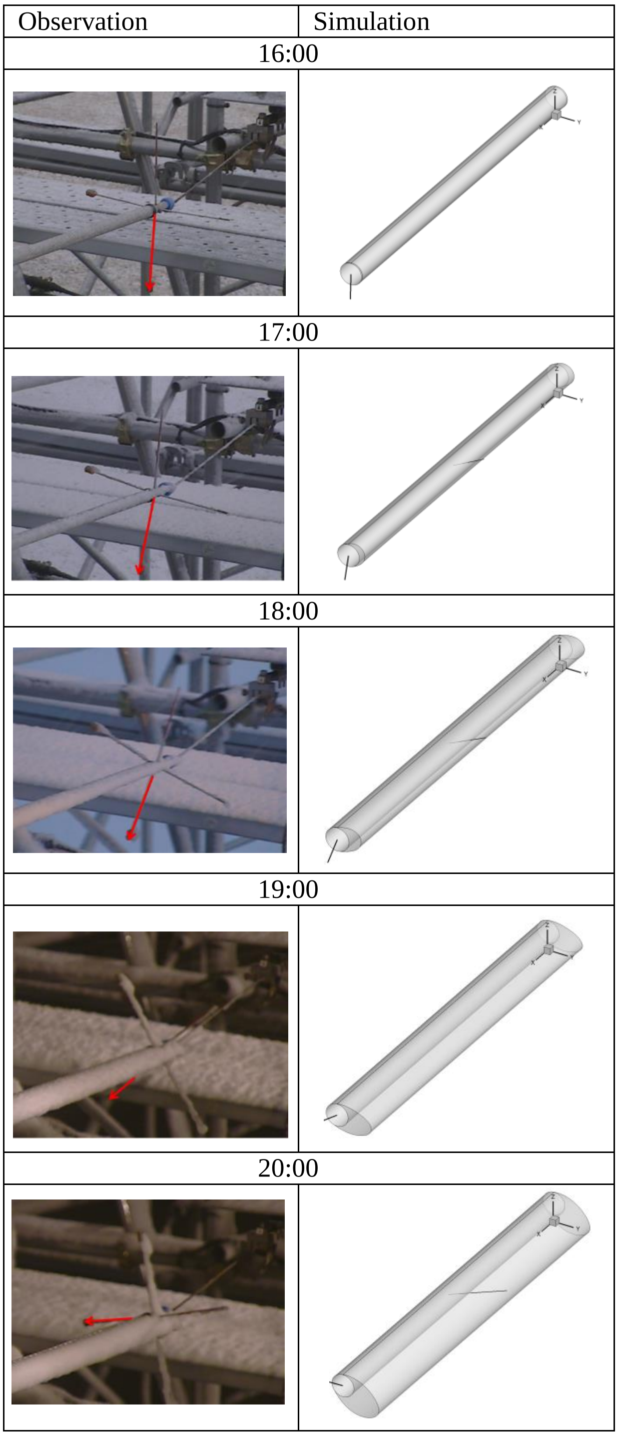

Fig.9 (a). Snow accretion process on sampler 1.

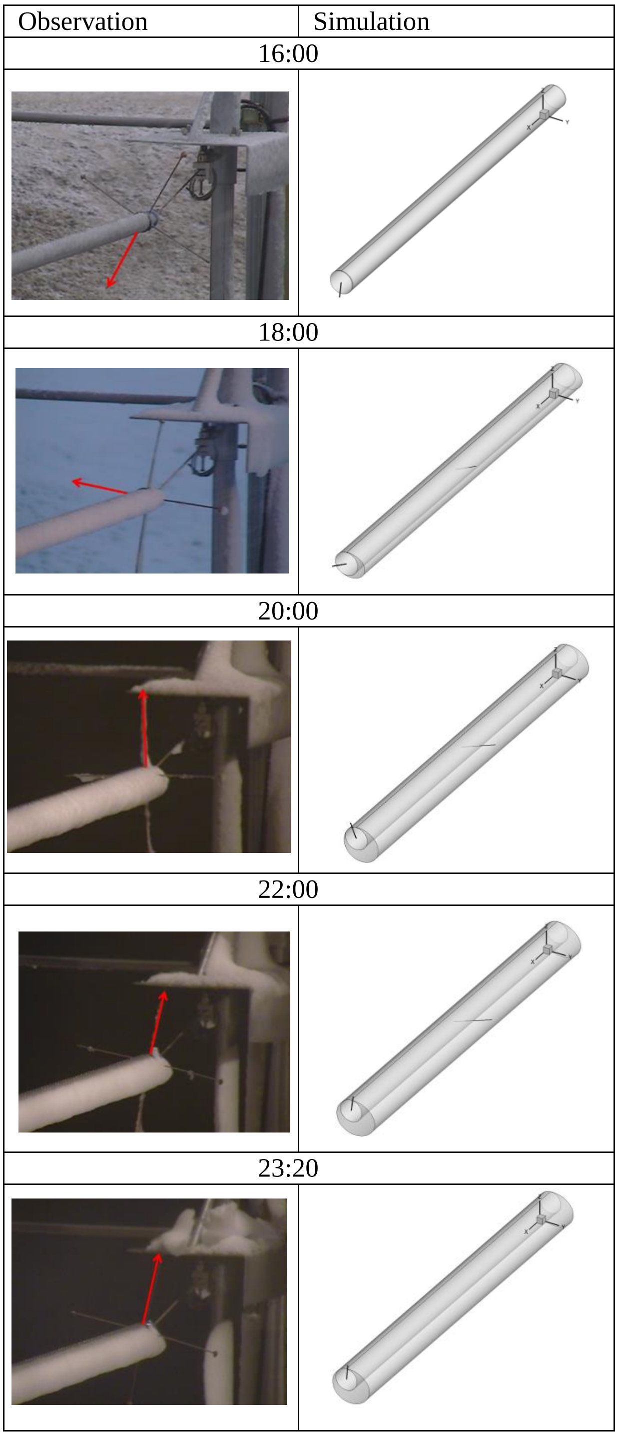

Fig.9 (b). Snow accretion process on sampler 2.

Analytical condition for numerical simulation using SNOVAL(Ver.3) is shown in Table1. The simulation was conducted for above conductor samplers with different size and torsion, but with the same direction relative to wind. Figure 11 shows the comparison of accreted snow mass numerically estimated with observations, as well as the cross section of calculated snow deposit. It is found that the growth rate of mass by simulation is consistent with the observations, especially the mass increased during 18:00~20:00 because of large impinging snow flux due to increased wind speed and precipitation rate.

The bold line on the section of snow deposit in Fig.11 indicates electric wire rotation from the initial position of 6 o'clock. This corresponds to conductor rotation which is estimated by measuring rotation angle of a rod attached on each side of a conductor sampler, as highlighted in red in Fig.9. Since the torsional spring constant of sampler 1 is greater than that of sampler 2, sampler 1 is hard to rotate and snow accumulation develops on the windward side. On the other hand, sampler 2 rotates easily compared to sampler 1 and the resulting accretion shape is close to a cylindrical-sleeve, except the top of electric wire is not completely covered with snow. The accreted mass on each sampler achieves a maximum, then the calculated rotation angle is roughly 90 [deg] for sampler 1, whereas 180 [deg] for sampler 2, which are agreement with the observations (see the rods highlighted in red in Fig.9).

The dashed and solid lines in Fig. 11 (a) are temporal change of accreted snow mass for different shear adhesive strength, $(\sigma_{sad})_{max} = 150[N/m^2]$ and $(\sigma_{sad})_{max} = 220[N/m^2]$,

Table1. Analytical condition

	Sampler 1	Sampler 2
type	ACSR 240 mm^2	ACSR 810mm^2
Sampler length L_x[m]	2	
Sampler diameter D_0[m]	0.0224	0.0384
Torsional stiffness GJ[Nm^2/rad]	68.8	588
Equivalent span length 2L[m]	90	300
Tosional spring constant $k_s/2$ [Nm/rad]	0.0680	0.0523
Azimuth θ_c [rad]	$\pi/8$	
Drag coefficient C_d	1.0	
Space division	Axial direction: 10 Circumferential direction: 720	
Time division [s]	1	
Time step	36000	
0℃ height of atmosphere [m]	250	
Initial radius of snowflake [m]	0.005	
Parameter in snow density ρ_0 [kg/m^3]	500	
Parameters in accretion factor A, B	0.38, 0.15	
Maximum of tensile adhesive strength $(\sigma_{tad})_{max}$ [N/m^2]	300, 360	
Maximum of shear adhesive strength $(\sigma_{sad})_{max}$ [N/m^2]	150, 220	

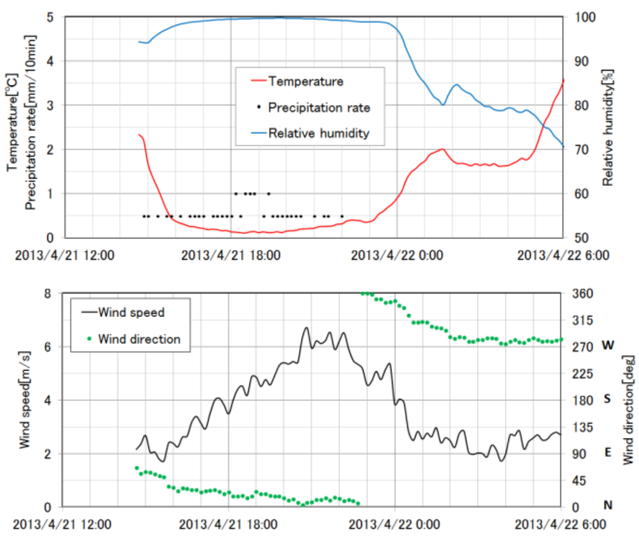

Fig.10. Meteorological data (top: temperature [℃], relative humidity [%], precipitation rate [mm/10min], bottom: 10min mean wind speed and direction).

respectively. The time of shedding for the latter coincides with the observation. However, the snow shedding model in SNOVAL(Ver.3) is based on shedding all at once, therefore, cannot explain a gradual decrease of accreted snow due to partial shedding after 20:30, as shown in the red line in Fig. 11 (a). The dashed and solid lines in Fig. 11 (b) are temporal change of accreted snow mass for different tensile adhesive strength, $(\sigma_{tad})_{max} = 300[N/m^2]$ and $(\sigma_{tad})_{max} = 360[N/m^2]$, respectively. The time of snow shedding in the former case is

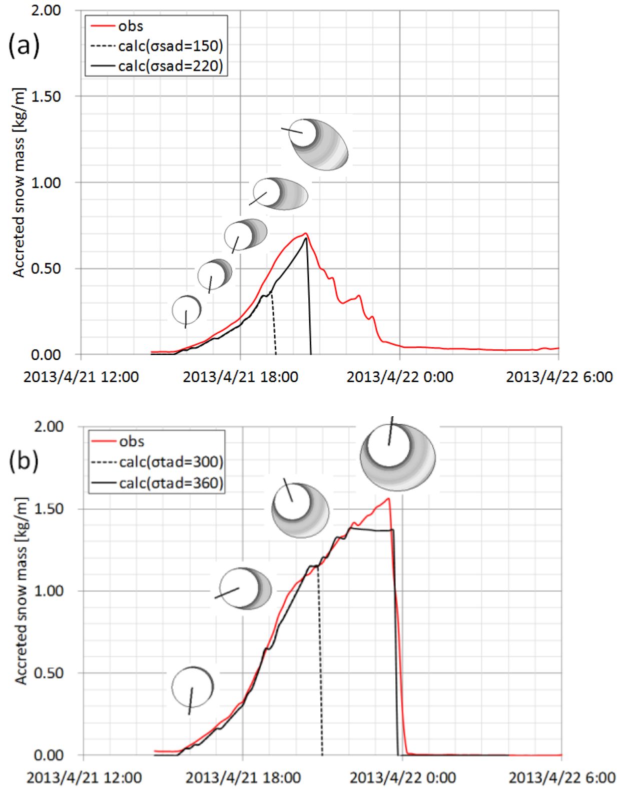

Fig.11. Comparison of observed with numerically estimated of accreted snow mass for different adhesive strength: (a) sampler 1, (b) sampler 2.

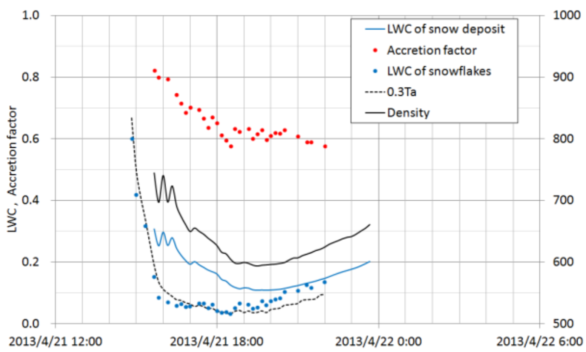

Fig.12. Temporal change of LWC of snowflakes before impact, accretion factor, LWC and density of snow deposit.

faster than the observation, whereas in the latter case, the time of shedding occurs at around the time of observed shedding.

Using the surface meteorological data and MANAL data on April 21, 2013, we calculate the LWC of snowflakes with initial radius of 5 mm and 0℃ height of atmosphere of 250m. Since the LWC of snowflakes and snow deposit is very sensitive to temperature variation, these temporal changes are reflected in Fig. 12. Indeed, the temporal change of LWC of snowflakes can be well approximated as $0.3T_a$. Mean LWC of snowflakes during 15:40~22:00 is about 0.08 and hence snowflakes prior to impact is expected to be sticky. Precipitation at observational location starts at 14:50. However, snow accretion does not occur until 15:40 because the LWC of snow deposit is over 0.4 and then adhesion force is zero (see Fig.8). Accordingly, SNOVAL(Ver.3) incorporating the model of snow accretion and melting can predict the start time of snow accretion. The temporal change of accretion factor and density of snow deposit is shown in Fig.12. It is found that the density is dominated by the change of LWC of snow deposit rather than that of wind speed. On the other hand, accretion factor decreases with decreasing the LWC of snowflakes and with increasing wind speed until 19:00, but after that the change is slightly suppressed due to the increase in the LWC of snowflakes. Mean values of accretion factor and density during snow accretion are 0.65 and $630[\mathrm{kg/m^3}]$, respectively. The latter is close to $660[\mathrm{kg/m^3}]$ estimated from the last image on Fig. 9(b).

III. Conclusion

The start time of snow accretion and the temporal change of mass and shape of accreted snow, wire rotation are evaluated using SNOVAL(Ver.3). They are consistent with field observations for conductor samplers supported by wires. However, the time of wet snow shedding strongly depends on the tensile and shear adhesive strength. It is necessary to estimate these strength experimentally for various LWC and density of snow deposit, and to consider the surface roughness of actual stranded wire. The findings from the analysis with SNOVAL (Ver.3) will be utilized to improve the accuracy in the estimation of accreted snow mass predicted by cylindrical-sleeve models and to predict snow deposit shape necessary for galloping analysis. In order for that, employing many wet snow events, the versatility of proposed accretion factor and density must be enhanced.

Acknowledgment

We would like to thank the Federation of Electric Power Companies of Japan for permitting us to use data obtained in the research for snow damage to overhead transmission and distribution facilities.

References

[1] G. Poots, *Ice and snow accretion on structures*, Research Studies Press, 1996.

[2] P. Admirat, “Wet snow accretion on overhead lines,” *Atmospheric Icing of Power Network*, Ed. M. Farzaneh, Springer, pp.119-169, 2008.

[3] Y. Sakamoto, “Snow accretion on overhead wires,” Phil. Trans. Roy. Soc. Lond. A., Ed. G. Poots, 358, pp.2941-2970, 2000.

[4] B. E. K. Nygaard et al., “Modeling Wet Snow Accretion on Power Lines: Improvements to Previous Methods Using 50 Years of Observations,” Journal of Applied Meteorology and Climatology, pp.2189-2203, 2013.

[5] K. Goto, “A Simulation Computation of Twist of De-Snowing Electric Wires due to Snow Accretion,” Seppyo, 38, pp.127-137, 2013.

[6] Y. Eguchi et al., “Development of simulation code SNOVAL for snow accretion on overhead transmission line-Formulation of snow accretion and growth models under oblique wind condition-” CRIEPI Research Report, No. N11016, pp.1-22, 2012.

[7] Y. Eguchi et al., “Development of a snow-accretion simulation method for transmission line under calm wind condition,” JSME annual meeting 2013, G01102.

[8] K. Ueno et al., “Development of models for snow accretion on electric wires and snow shedding with melting process,” CRIEPI Research Report, No. N15001, pp.1-29, 2015.

[9] T. Matsuo and Y. Sasyo, “Melting of snowflakes below freezing level in the atmosphere,” J. Meteorol. Soc. Jpn. 59, pp.10-25, 1981.

[10] R. Hefny et al., “Adhesion of wet snow to different cable surfaces,” Proc of the 13th International Workshop on Atmospheric Icing of Structures, Andermatt, Switzerland, 2009.

[11] K. Sato, “Snow cap and accretion phenomena due to wet snow,” Workshop of reserch for radar and numerical model on precipitation, 2014.

[12] T. Nishihara et al., “Study of Damage to Overhead Trasmission Facilities Caused by Wind, Snow and Salt -Research results in fiscal years 2007－2011-,” CRIEPI Research Report, No. N19, pp.1-130, 2013.

[13] H. Schlichting and K. Gersten, *Boundary Layer Theory*, Springer, 1999.

[14] A. Sato and G. Wakahama, “Adhesion force of wet snow,” The Japanese Society of Snow and Ice autumn meeting, p.111, 1974.

[15] Y. Mizuno and G. Wakahama, “Adhesive Strength of Wet Snow,” Low Temperature Science, Ser. A, 35, pp.133-145, 1977.

[16] T. Nishihara et al., “Development of a simple device for observing snow accretion by using a short dummy conductor supported by wire ropes,” CRIEPI Research Report, No. N11030, pp.1-17, 2012.